Kinetics of the aqueous-ethanol solution mediated transformation between the beta and alpha polymorphs of para-aminobenzoic acid

Thomas D. Turner*, Steve Caddick, Robert B. Hammond, Kevin J. Roberts and Xiaojun Lai

School of Chemical and Process Engineering, University of Leeds, Woodhouse Lane, Leeds, LS2 9JT

* Corresponding Author

1

Abstract

A quantitative kinetics analysis of the solution-mediated phase transformations in aqueous-ethanol between the enantiotropically related alpha and beta polymorphs of para-aminobenzoic acid (PABA) is presented. A new temperature-controlled transmission flow-cell design for use with a laboratory X-ray source which can be utilised for diffraction or scattering experiments is described. This transmission cell in combination with in-situ slurry X-ray diffraction is utilised to provide a quantitative analysis of the percentage by mass of respective solid phases in flowing suspensions, coupled with solution concentration as measured with UV-Vis spectroscopy. The separate phases are identified through individual fingerprint peaks, the (1 0 3) reflection at $2\theta = 15.6°$ relating to the alpha phase and the (0 2 2) reflection at $2\theta = 25.3°$ for the beta phase. Examination of the conversion of a slurry of beta PABA in a 70:30 water:ethanol solvent mixture to the alpha polymorph, at a temperature range of 24-30°C reveals the rate of dissolution of the beta phase is consistent with zero order kinetics (rate constant $k_{d\beta}$ $6.80\times10^{-4} - 8.17\times10^{-5}$ wt% s^{-1}) , while the growth of the alpha phase follows first order kinetics ($k_{g\alpha}$ $1.00\times10^{-3} - 2.50\times10^{-4}$ w% s^{-1}). Extrapolation of the growth and dissolution rate constants yields a transformation temperature for the phase inter-conversion of 22-24 °C. Overall the data is consistent with a fast de-supersaturation of the solution concentration indicating a dissolution-controlled polymorphic transformation process.

1. Introduction

Polymorphism is a property exhibited by many organic molecules whereby a single chemical entity can pack in crystallographically different forms; these forms are the same compound but may have very different physicochemical properties[1][2]. Polymorphism is of specific interest to the pharmaceutical sector due to the sometimes catastrophic effects small changes in molecular assembly have on the physical or chemical properties of a material. The influence of downstream processing complications, solubility variations, bio-availability, reactivity and performance issues of pharmaceutical and small organic molecules due to unwanted polymorphic changes have been well documented[3]. A classic example is Ritonivir where a change in the known polymorphic form led to a fourfold reduction in material solubility resulting in product withdrawal[4]. A number of other examples have been discussed by Dunnitz and Bernstein[5], which has sought to highlight the difficulty of polymorphic control during the preparation of some organic materials. Transformation between polymorphic forms are often solution mediated[6] and the thermodynamic and kinetic factors governing such transformations are important if a process is to be, not only fully understood and characterised, but also if it is to be controlled in a reproducible manner. The kinetics of polymorphic phase transformations can be monitored offline through the use of sampling methods together with crystal characterisation using e.g. X-Ray diffraction (XRD), Raman spectroscopy, differential scanning calorimetry and particle size/shape analysis[7][8]. However a step towards fast, online methodologies for monitoring crystallisation parameters in-situ which can be transferable to various scale sizes is needed in the industrial sector not only as a means of cost reduction but also in order to reduce sampling errors[9].This desire for online monitoring of crystallisation processes in an attempt to control unwanted phase transitions has led to an increase of research into this area as well as the development of numerous online monitoring techniques. A number of studies have implemented the use of in-situ

3

Raman spectroscopy probes to monitor the polymorphic phase inter-conversion of organic crystal systems, along with various techniques to quantify solution concentration such as UV-Vis spectroscopy and FTIR spectroscopy [10] [11] [12] [13] [14] [15].

The attraction of monitoring a materials polymorphism for solid form and hence purity control during crystallisation processes in the pharmaceuticals and materials industry, has led to the development of in-situ XRD characterisation. Previous work using flow cells, plug flow reactors and static melt crystallisation cells on lab sources and at synchrotron sites have shown the benefits of in-situ measurements to yield information on initial polymorphic forms in crystallising systems and nano-structural characteristics during nucleation events[16] [17] [18] [19] [20] [21] [22] [23] [24] [25] [26]. In-situ XRD has also shown to be a useful tool in quantitative analysis and phase inter-conversion kinetics through peak integration methods[27] [28].

This study focuses on the phase transformation of the two polymorphic forms of p-Aminobenzoic Acid (PABA) which has two enantiotropically-related polymorphs, alpha and beta. The alpha crystal structure is monoclinic and has the space group $P2_1/n$ with 2 crystallographically independent molecules in the asymmetric unit with 4 asymmetric units with unit cell dimensions a = 18.551, b = 3.860, c = 18.642 Å, with a beta angle = 93.56°[29]. The beta form crystallises also in the monoclinic system but in the space group $P2_1/c$ and with a uni-molecular asymmetric unit having 4 molecules in a unit cell of dimensions a = 6.275 Å, b = 8.55 Å, c = 12.80 Å, and a beta angle = 108.30° [30]. The system transition temperature has been previously quoted as 22°C, as obtained from solubility data[31], whereas a more recent study[32] using in-situ Raman spectroscopy quoted a value of 13.8°C. In both cases the alpha form been the form stable at higher temperatures whereas the beta form is stable at lower temperatures. The alpha form crystal structure contains a dominant OH-O carboxylic acid dimer and π-π stacking interactions which contribute considerably to the lattice energy[33]. The alpha form is generally crystallised more readily under kinetic

4

conditions which has been linked to the possible formation of the COOH dimer, inherent within the alpha structure, in the solution phase[34] [35]. The beta form lacks this dimer been characterised by a four membered NH-O and OH-N hydrogen bonding ring[33]. The commercially available alpha polymorph is of a needle morphology and the beta polymorph is of prismatic morphology[36]. Comprehensive nucleation kinetics of the alpha form of PABA have recently been reported; utilising both isothermal and poly-thermal approaches to understand molecular de-solvation during the nucleation process and the impact of solution supersaturation on nucleation mechanism[34, 37].

This paper presents an examination of the solution-mediated polymorphic inter-conversion of the beta to alpha forms of PABA utilising a new experimental set-up encompassing transmission XRD slurry flow cell used in combination with solution concentration measurements using ATR UV/Vis spectroscopy. The data is analysed resulting in the derivation of the transformation kinetic parameters together with a detailed analysis of the rate-determining steps involved as obtained through a comparison of the solids and solution concentration transformation profiles.

2. Materials and Methods

2.1 Materials

The PABA used in this study was supplied by Sigma Aldrich with a purity of >99%, ethanol was used as supplied by Sigma Aldrich at 98% purity, deionised water was also used in calibration and preparation of the beta form crystals.

2.2 Preparation of Starting Materials

The crystals of the beta polymorph were prepared using an isothermal slurry inter-conversion method from the alpha form at 5°C over a period of ca. >10 days. Typically a 10 w/w% slurry of alpha form crystals were prepared in deionised water a magnetically stirred (300 rpm) 200ml scale jacketed batch reactor, temperature control of the system was provided by a Julabo[38] F32 oil bath using a Pt100 resistance probe. The inter-conversion process was analysed off-line using a Bruker D8[39] diffractometer for powder X-ray diffraction (PXRD) analysis, in order to determine the alpha and beta phase solids concentration to ensure the polymorphic purity of the resulting beta phase crystals. Samples of slurry were taken, filtered under vacuum and dried immediately in a sample oven set at 60°C for 12hours, the dried sample was then analysed by PXRD and full profile fitting carried out determine sample purity. Seed crystals of the alpha form for the transformation experiments were prepared using PABA as supplied by Sigma, the material was milled using a mortar and pestle to a particle size of ca. 50 μm by optical microscopy.

2.3 In-Situ PXRD System and Flow Cell

The general experimental set up for the in-situ XRD analysis has been previously described in some detail [28] [40] [41]. In summary, it comprises an INEL[42] 120° curve position sensitive detector, Bede[43] Microsource X-ray generator (Cu K-alpha) with a mono-chromator, X-ray

beam conditioning slits and collimator set within a safety enclosure. The slurry flow through system comprised a 100ml jacketed glass crystalliser, where agitation was provided by magnetic stirring and temperature monitoring of the reactor contents temperature was carried out using a Pt100 probe connected to a Julabo[38] F32 circulation bath.

A new in-situ X-ray transmission flow-through cell was designed, constructed and employed onto the existing system as shown in Figure 1a) and b). The cell contains a cartridge with a borosilicate glass capillary tube secured inside, this permits the X-ray beam to impinge upon the crystals within the flowing slurry, a full description of the transmission cell can be found in S1 in the supporting information. This in-situ cell was commissioned before use in the transformation experiments and was found to produce a limit of detection, i.e. the least amount of material before detection at the detector, of ~0.6 wt% for the alpha polymorph, details of the commissioning experiments are provided in S2 in the supporting information.

The in-situ cell and slurry flow cell flow lines were temperature-controlled via coaxial hose fittings, this allowed the same cooling/heating liquid within the circulation bath used for the reactor to be supplied to the flow-through cell to minimise temperature variations between the reactor and cell. A flow loop was used between the reactor and cell to enable circulation of the crystal slurry with flow enabled using a Watson Marlow[44] 300 series peristaltic pump. The concentration of the solution was monitored within the batch reactor using a Zeiss MCS621 [45] UV-VIS spectrometer equipped with an ATR probe. A multi-channel analyser was utilised to read the detector signal together with Bede[46] software; Polycrystal[43], for analysis of the collected XRD profiles. A PC with National Instruments LabVIEW[47] software was used to collect data for the UV-Vis spectrometer as well as control the reactor and monitor the temperature profiles.
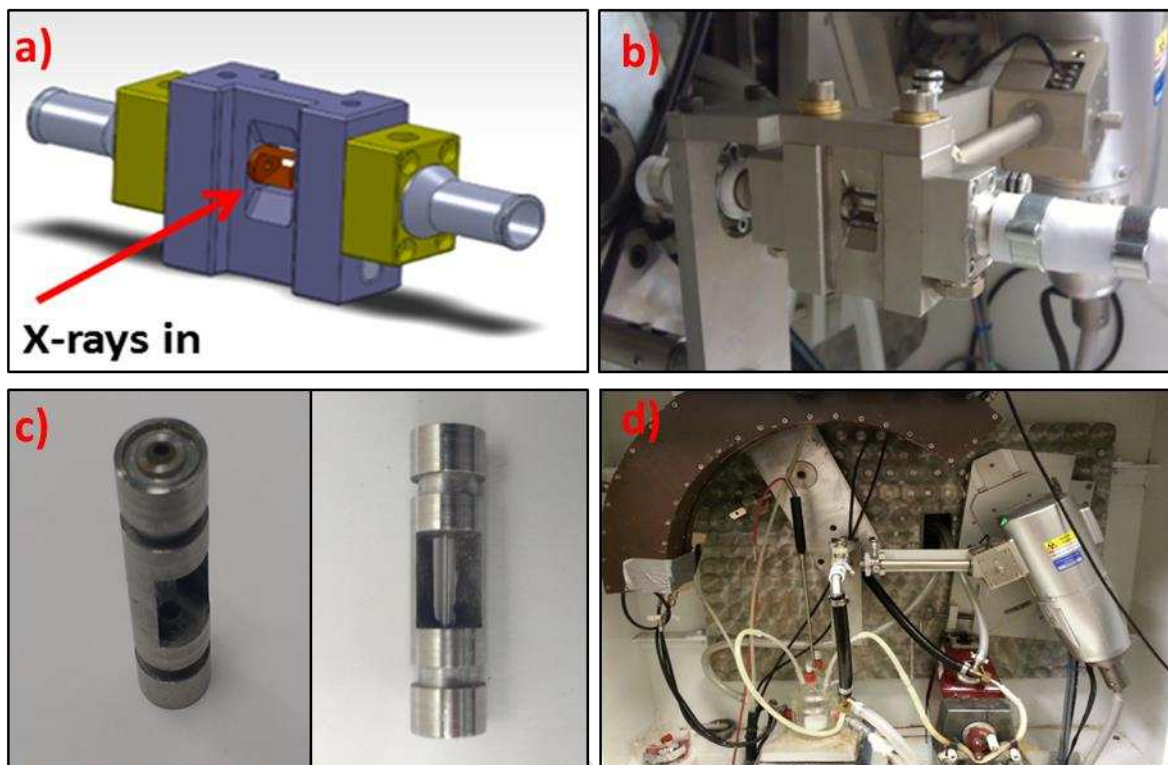
Figure 1a) A drawing of the new transmission X-ray flow through cell, b) the new cell positioned within the X-ray enclosure set-up in transmission mode with the X-ray source in the background, c) replaceable flow cell cartridges with borosilicate glass windows, d) Experimental setup of the online XRD unit, highlighting the curved detector, x-ray source, reactor and flow cell and flow cell

2.4 Polymorph Concentration Calibration in Crystal Slurries

The solids concentration of each polymorph in a crystalline slurry was related to the area underneath a significant peak in the diffraction pattern for the two polymorphs. A saturated solution of the alpha or beta polymorph in 70:30 deionised water : ethanol, was prepared and held at 20°C, in the case of beta this prevented any transformation to the alpha form as at this temperature the transformation is sufficiently slow. This solvent mix was used as PABA is hydrophobic hence mixing with pure water causes the slurry to foam and separate, 70:30 water:ethanol mixes provided a low volatility and also sufficient mixing of the solid and solution phases to produce a homogenous slurry. The solids concentrations of separate alpha

and beta slurries analysed were 2, 4, 6, 8 and 10 wt% where the XRD data collection times were 5 minutes.

2.5 Polymorphic Slurry Transformation Experiments

The solubility of the alpha polymorph was determined by gravimetric analysis, a full description of the method and data is provided in S3 in the supporting information. A saturated solution of beta PABA was prepared in the chosen 70:30 water:ethanol solvent established from existing solubility data for the alpha polymorph and adding small amounts of beta PABA to the saturation concentration at the specified isothermal temperatures; 24, 26, 28, 30, 32, 34°C. A slurry containing 7 wt/wt% solids of the beta polymorph was prepared with agitation at 300 rpm provided by magnetic stirring. Seeded crystallisation experiments were carried out to ensure data collected reflected the dissolution and growth processes mindful that low temperature un-seeded experiments can take several days to transform due to the long induction time for spontaneous nucleation. Following this, 0.2 wt/wt% of alpha form seeds were added to the reactor and XRD patterns were recorded at 300 second intervals. The solution concentration was monitored by recording the UV/Vis absorbance of the reactor contents every 300 seconds from a UV/Vis ATR probe in the vessel.

2.6 Data Analysis

The XRD data collected was smoothed using smoothed principal component analysis (SPCA) with a purpose written algorithm[48] which improved the signal to noise ratio of the patterns and hence provided a lower limit of detection for the two polymorphic forms. The smoothed data were analysed using the software package Polycrystal[43], which involved background subtraction through an iterative process to provide an estimation of the background scattering of X-rays by air, the solvent and the borosilicate glass of the cell. The reduced patterns were then analysed by performing a peak searching function through a standard deviation method

to identify peak position, followed by application of a Gaussian function to calculate a fitted peak area, this value was used to relate the solid concentration of the slurry (wt %) to the recorded diffraction patterns. A comprehensive review of this methodology is provided in Dharmayat et al (2008)[28].

The growth and dissolution processes of SMPT for the two solid phases were further analysed through application of simple reaction models. This was achieved by converting the calculated wt/wt% from the calibration models to the fractional conversion of solids for each phase using Equations 1 and 2.

$$X\beta = 1 - \left(C\beta(t) \middle/ C\beta(i) \right) \quad \textbf{(Equation 1)}$$

$$X\alpha = C\alpha(t) \middle/ C\alpha(f) \quad \textbf{(Equation 2)}$$

Where $C_\alpha(t)$ and $C_\beta(t)$ are the concentrations of the respective phases at a given point in the reaction, $C_\alpha(f)$ and $C_\beta(i)$ are the concentration of alpha phase formed at the end of the reaction and the initial starting concentration of the beta phase respectively, $X\alpha$ and $X\beta$ are the fractional conversions of the alpha and beta phases respectively.

$$k_{d\beta}t = X\beta \quad \textbf{(Equation 3)}$$

$$k_{g\alpha}t = -\ln(1 - X\alpha) \quad \textbf{(Equation 4)}$$

The dissolution and growth profiles were fitted to zero and first order equations respectively as highlighted in Equations 3 and 4, where $k_{g\alpha}$ is the growth rate constant with respect to the alpha polymorph, $k_{d\beta}$ is the dissolution rate constant with respect to the beta polymorph and t is time.

3. Results and Discussion
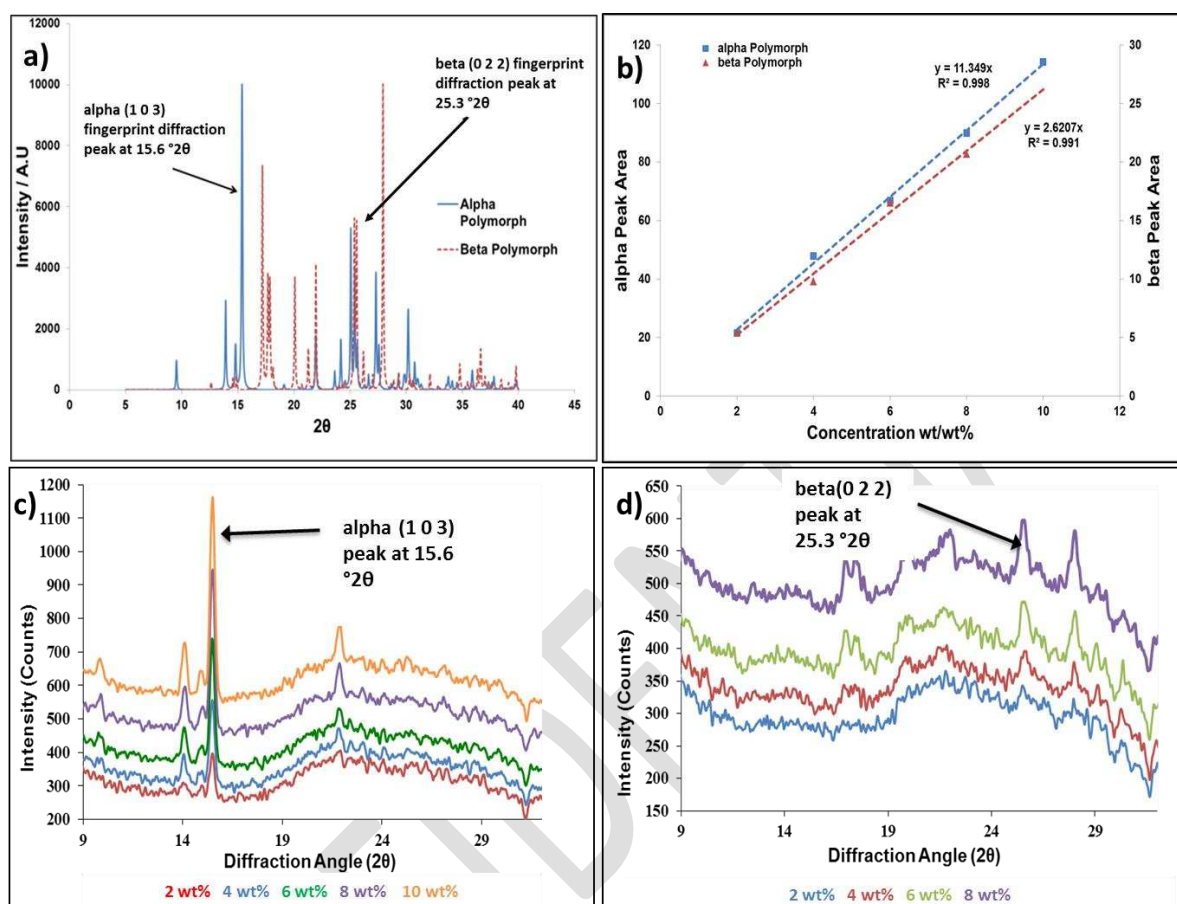
3.1. Solid Phase Concentration Calibration

Figure 2 a) Modelled PXRD patterns from the crystal structures of both polymorphs highlighting the fingerprint peaks of both polymorphs, b) The calibration of peak area to concentration in wt/wt% of the alpha (1 0 3) and beta (0 2 2) fingerprint peaks c) Diffraction patterns as a function of slurry concentration for the alpha polymorph and d) The beta polymorph

A comparative examination of the reference XRD patterns for the alpha and beta phases, as shown in Figure 2a) reveal suitable finger printing X-ray peaks for solid phase concentration calibration. In this the (1 0 3) and the (0 2 2) peaks for the alpha and beta forms respectively, were found to be the most suitable, i.e. being free from competing (overlapping) peaks of the other phase. This was aided by the preferential orientation of the needle-like alpha crystals within the slurry line which reduced greatly the higher order diffraction peak intensity of this phase. From measurement of the peak areas of the (1 0 3) and (0 2 2) fingerprinting peaks as

a function of concentration, Figure 2c) and d) respectively, the solid concentrations of the two phases could be calculated by using calibration curves as shown in Figure 2b).

3.2. Phase Transformation from Unseeded and Seeded Slurries

It should be noted that the higher temperature seeded experiments at 32 and 34°C and unseeded experiments at 35°C and 45°C were not considered in this analysis as the conversion rate was found to be too high relative to the data collection time resulting in a limited number of data points and thus extrapolation of kinetic parameters was not possible. The raw conversion data for these higher temperature seeded and unseeded experiments can be found in S4 and S5 in the supporting information respectively.

Figure 3a) shows overlaid time-dependant XRD data for the seeded phase transformation between the beta and alpha polymorphs at 30°C, the data is staggered with time along the y axis for clarity. The finger-printing (1 0 3) alpha and (0 2 2) beta peaks can be clearly seen revealing that the dissolution of the beta phase occurs rapidly followed by growth of the alpha phase. Figure 3b) shows the data at the lower temperature of 24°C where the major beta peaks are still visible however it can be seen that dissolution and growth at this lower temperature happens much less rapidly.
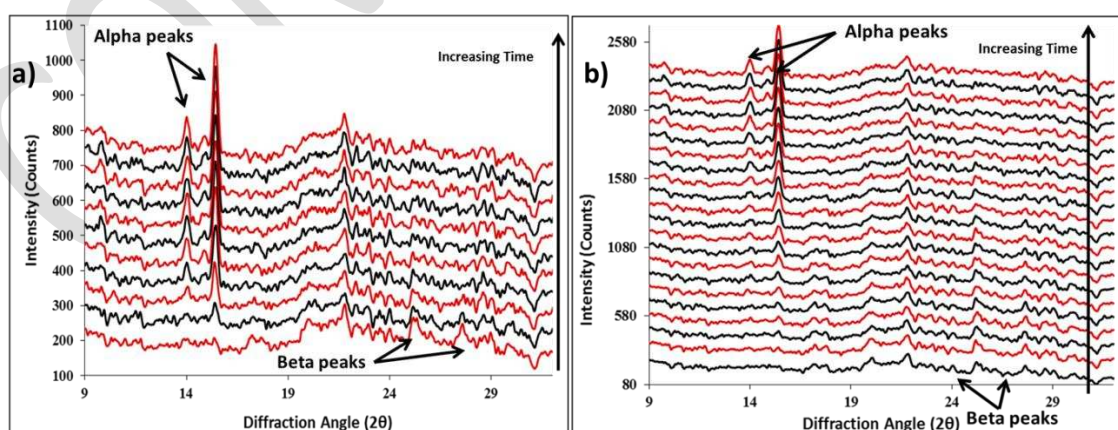

Figure 3 a) The recorded diffraction patterns, each a five minute data collection time, for the seeded SMPT of beta to alpha phases at 30°C as a function of time, b) the collected diffraction patterns for the SMPT at 24°C

3.3. Determination of Kinetic Parameters

Figure 4a) shows the fraction of solids converted of each phase for the seeded slurry transformation experiment carried out at 30°C, this analysis was carried out for each isothermal experiment. The dissolution of the beta phase was found to follow a zero order model using Equation 3, this highlights that the beta phase dissolves very quickly at the beginning of the SMPT to provide the necessary supersaturation for the fast growing alpha phase. The growth profiles of the alpha phase, were seen to fit a first-order model using Equation 4, in good agreement with previous studies for the growing phase during the polymorphic transformation of L-glutamic acid[28]. Fitting of the growth and dissolution profiles using these simple kinetics models allows the extrapolation of the rate constants associated with each process to determine which is rate-limiting in the transformation kinetics.
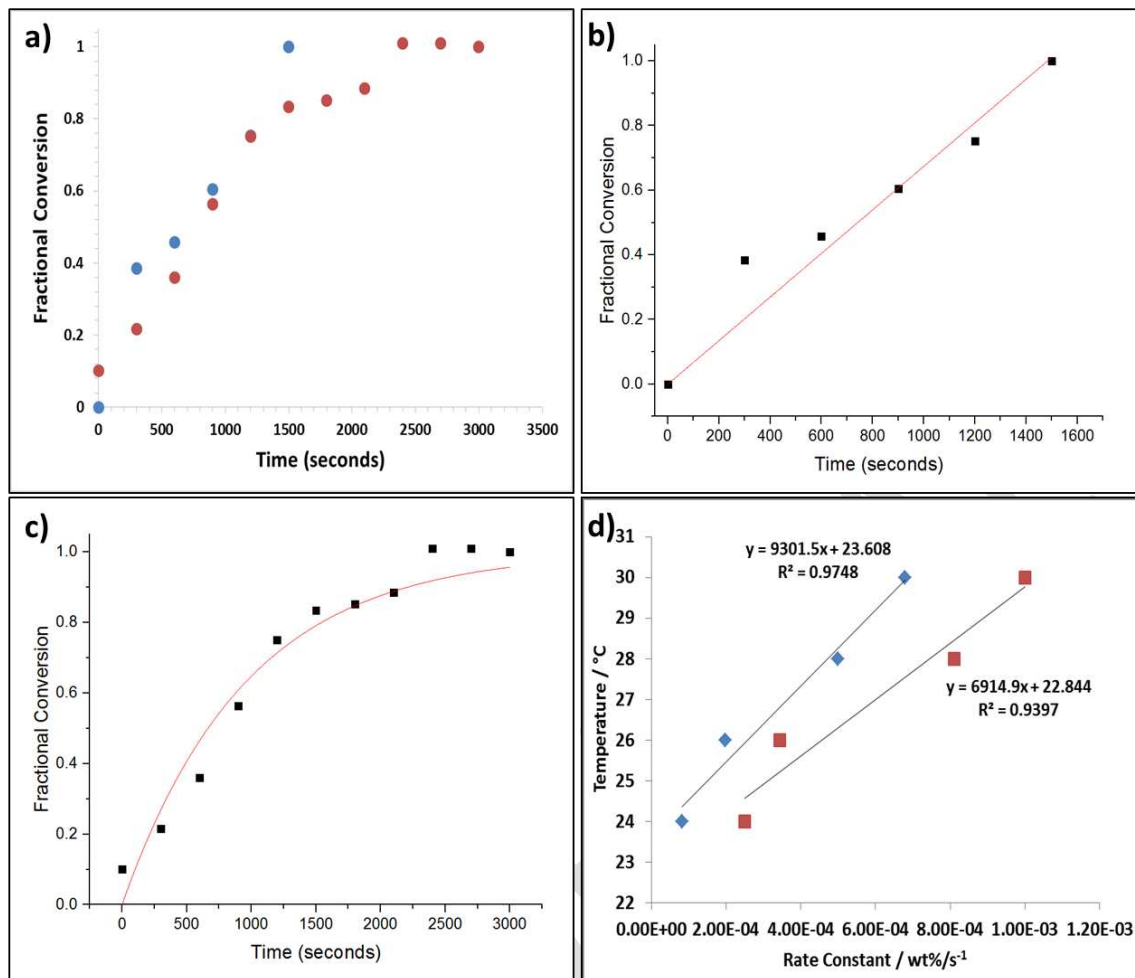
Figure 4 a) The SMPT at 30°C indicating the fractional conversion of solids in the slurry, red circles: fractional conversion of beta phase, blue squares: fractional conversion of alpha phase, b) dissolution of beta phase solids with zero order fit c) growth of alpha phase with first order fit, d) growth rate constants (red squares) and dissolution rate constants (blue diamonds) as a function of experimental isothermal temperature

The dissolution of the beta solids and the growth of the alpha solids together with the zero and first order fitting profiles are highlighted in Figure 4 b) and c), the calculated values of growth and dissolution rate constants from the fitting process as a function of the isothermal temperature are provided in Table 1. The error of these measurements was assessed by repetition of the 28°C isothermal experiment and calculating the growth and dissolution rate constants, $k_{g\alpha}$ and $k_{d\beta}$ respectively, over six separate repetitions. The standard deviation was found to be 8.8% for $k_{g\alpha}$ and 12.6% for $k_{d\beta}$, which gave confidence to the calculated values at

other temperatures, a full description of the error calculation can be found in S6 in the supporting information. Further to this a note should be made about the solution absorbance measurements which were recorded for each single experiment and no repetitions were carried out in this regard, as such care should be taken when analysing these data as the solubility of the two polymorphs are very close.

The growth profiles of the alpha phase, highlighted in Figure 4c), indicate that although a simple first order model can be used to fit this curve, there is some deviation from the model; particularly at the beginning of the experiment and towards the end of the growth process. This initial deviation is likely due to the slow initial growth of the alpha phase due to poor supersaturation generation by the slowly dissolving beta phase. The deviation from the fitted model towards the end of the process is likely caused by poor mass transfer of solute molecules from the almost supersaturation depleted solution, to the growing alpha crystals.

Table 1 The calculated dissolution and growth rate constants and their ratios for the isothermal experiments

Temperature (°C)	$k_{g\alpha}$ (wt% s^{-1})	$k_{d\beta}$ (wt% s^{-1})	$k_{d\beta}/k_{g\alpha}$
24	2.50E-04	8.17E-05	0.33
26	3.43E-04	1.98E-04	0.58
28	8.11E-04	4.99E-04	0.62
30	1.00E-03	6.80E-04	0.68

3.4. Estimation of the Enantiotropic Phase Transition Temperature

Figure 4d) provides a plot of the dissolution and growth constants derived from the fitting process of the reaction models to the transformation profiles as a function of temperature. The data provide an estimation as to the polymorphic transition temperature through extrapolation of the two constants to 0 wt% / s^{-1}. The dissolution and growth rate constants were fitted with a linear function of the form y = 9301.5x + 23.608 R^2 = 0.98 and y = 6914.9x

+ 22.844 R^2 = 0.94 respectively. The two equations provide an upper and lower estimate of the transition temperature for this enantiotropic system as 22.8 – 23.6 °C.

Previous calculations of the transition temperature for the two polymorphs of PABA, both from solubility measurements, were found to be 25°C and 16°C by Gracin et al and Svard et al, agreeing well with the value calculated in this work[31 49]. The reason for the variation in the two quoted values from previous work is due to the close proximity of the alpha and beta solubility lines, and hence identifying an enantiotropic transition point is susceptible to systematic errors. A further study which utilised in-situ Raman spectroscopy to monitor the solids concentrations of two polymorphs by Hao et al[32], found the transition temperature to be 13.8°C. The differences in this reported value and the in-situ XRD measurements in this work, may be due to timescale differences of the experiments, hours in the XRD experiments and days for the Raman experiments.

Table 2 the current literature measurements of the enantiotropic phase transformation temperature for PABA

Transition Temperature	Experimental Method	Reference
25 °C	Solubility Measurement	Gracin et al[31]
16 °C	Solubility Measurement	Svard et al[49]
13.8 °C	in-situ Raman Spectroscopy	Hao et al[32]
22.8-23.6 °C	in-situ XRD	This Research

The XRD experiments presented here did not characterise lower temperatures for transformation due to timescale limitations of the experimental set-up for long data collection

times. Additionally measurement of the alpha to beta transformation could shed more light on the transformation process, however this reverse transformation requires weeks at low temperatures and as such suffers the same timescale limitations from the current experimental set-up. Furthermore higher temperature unseeded experiments were carried out to try to assess the impact of nucleation times on the inter-conversion process however at the 35 and 45°C the interconversion occurred too rapidly for fitting of kinetic models to the data, full details can be found in S5 supporting information. This was due to long data collection times of 5 minutes of the laboratory XRD and hence future work to characterise this phase interconversion process at higher temperatures could be carried out using high flux synchrotron radiation facilities.

3.5. Analysis of Time-Dependant Solution and Solids Composition

The SMPT of two solid phases can be described, in terms of the overall rate of transformation, as the nucleation of the stable form (alpha in this case) the dissolution rate of the metastable form (beta in this case) and growth of the stable form. From the calibrated in-situ XRD measurements the relative time-dependant concentrations of the two polymorphs as a function of temperature has now been determined. These can be combined with the measured UV/Vis absorbance which is related to solution concentration of PABA, and hence the analysis of these three components can be described.
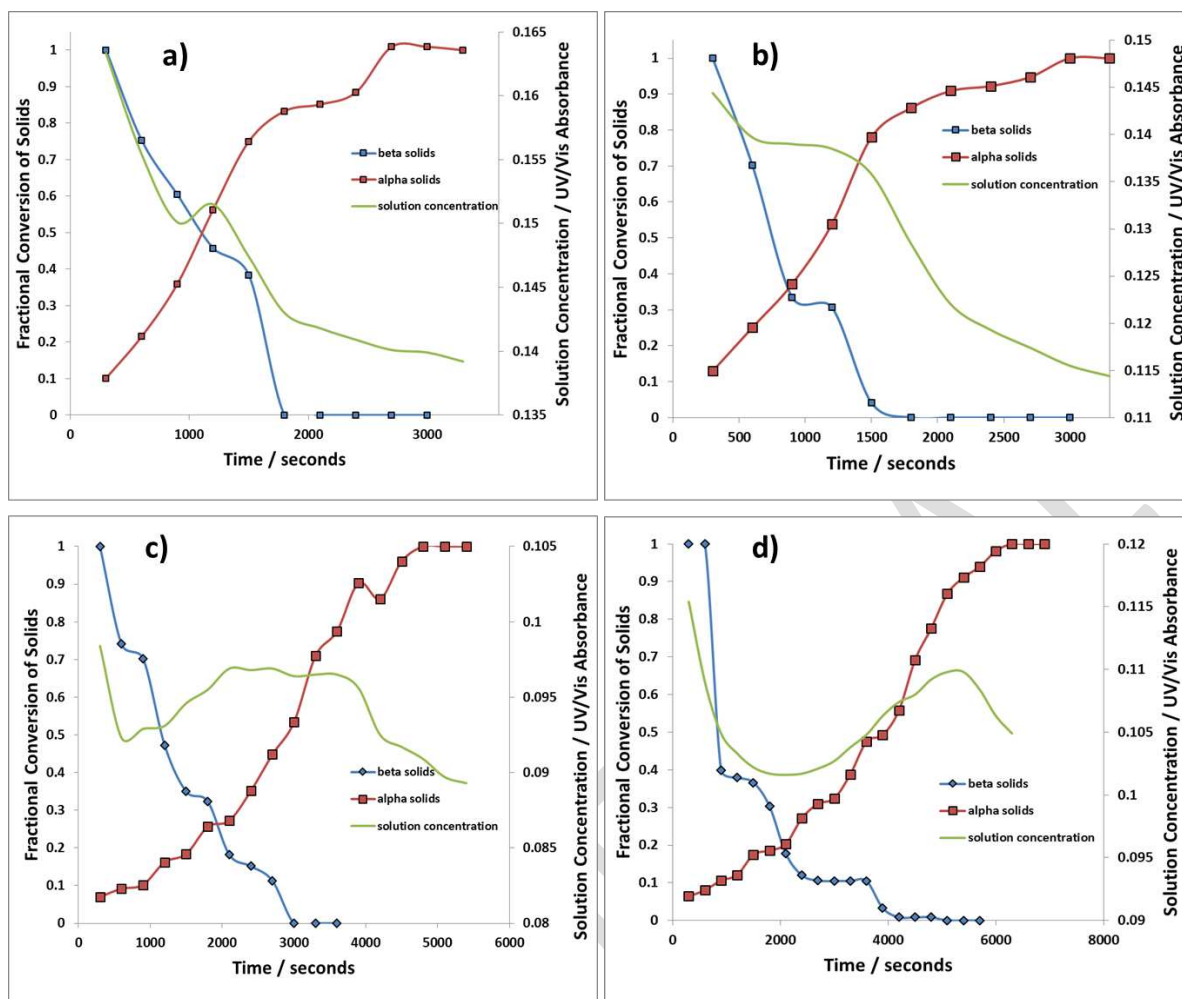
Figure 5 beta to alpha phase transformation profiles at a) 30°C, b) 28°C, c) 26°C and d) 24°C, highlighting the fractional conversion of the solid phases together with the measured UV-Vis absorbance of the solution

Figure 5 merges the calculated fractional conversion of the solids concentrations of the alpha and beta forms of PABA, with the measured solution concentration with respect to the absorbance measured from UV-Vis analysis. It should be noted that the ratios of the solid phase concentrations do not always equal 1 during the phase transformation, this was attributed to two components; the first was the preferential orientation of the needle like crystals of the alpha phase producing a strong diffraction signal of the (1 0 3) peak and also the poor diffraction of the beta phase relative to alpha which becomes particularly notable at low beta solids concentrations.

18

From analysis of the solids concentration profiles it is evident that all the SMPT experiments proceeded with a sharp reduction in the overall solids concentration of the metastable beta phase. This observation indicates that the nucleation rate of the stable form is very high, this is unsurprising as these experiments were carried out under seeding conditions, further to this the solution was supersaturated with respect to the metastable beta phase and hence the supply of secondary nuclei combined with a low thermodynamic and kinetic barrier to nucleation results in high nucleation and growth rates.

The trend in solution absorbance as measured by UV/Vis spectroscopy was found to be quite similar for all 4 isothermal temperatures where the solution de-supersaturated very rapidly at the start of the transformation process. This de-supersaturation of the solution largely precedes the nucleation and growth of the alpha phase and also the rapid dissolution of the beta phase. This suggests that the SMPT is a 'dissolution controlled' process (Figure 5) where the rate of formation of the stable phase or growth rate of alpha ($\%$wt.s^{-1}) is much larger than the dissolution rate of the metastable beta phase ($\%$wt.s^{-1}) required to maintain the relative supersaturation in the system.

The ratios of the calculated dissolution and growth rate constants, summarised in Table 4, also support this conclusion where the values at all isothermal conditions are <1. This is supported by the previous work of Davey and Cardew[50] who highlighted that a dissolution controlled process results in this ratio becoming less than 1. This observed dramatic decrease in solution absorbance is proceeded by a plateau phase in the transformation, this is visible in the experiment carried out at 28°C in Figure 5b). An explanation for this is that an equilibrium point is reached in the transformation process where the combination of the very fast nucleation and subsequent growth of alpha with the slow dissolution of beta becomes rate limiting.

19

3.6. Factors Influencing the Kinetics of the Transformation Process

A number of factors could potentially impact the relative rate processes involved in the transformation process and these have been highlighted by O'Mahony et al[7], when comparing the phase transformation profiles of a number of organic materials. Conventionally the rate of dissolution $(g/m^2.L.s)$ is usually assumed to be greater than the rate of growth $(g/m^2.L.s)$. This reflects the fact that the latter involves transport of solute across a boundary layer followed by molecular rearrangement at the surface and subsequent integration to kink sites[7]. In the current study it has been shown that it is the dissolution of the metastable beta phase that is the rate determining step during the SMPT of the beta to the alpha polymorph. This observation has also been reported for the case DL-methionine during the SMPT of the α to γ polymorph, where the dissolution of the metastable α form was found to be rate limiting[51].

This dissolution controlled process may be influenced by the observed experimental particle morphology for the two polymorphs, with the beta phase being prismatic and thus much more isotropic in shape in comparison to the more needle-like morphology of the alpha polymorph[33, 36] as shown in Figure 6. These differences would be consistent with a slower dissolution rate for the prismatic beta phase due to smaller solid-liquid interfacial surface area per volume mass relative to the very directional growth of the needle-like alpha phase, which primarily occurs along the b axis and has a much larger solid-liquid interfacial surface area per unit mass of crystals.
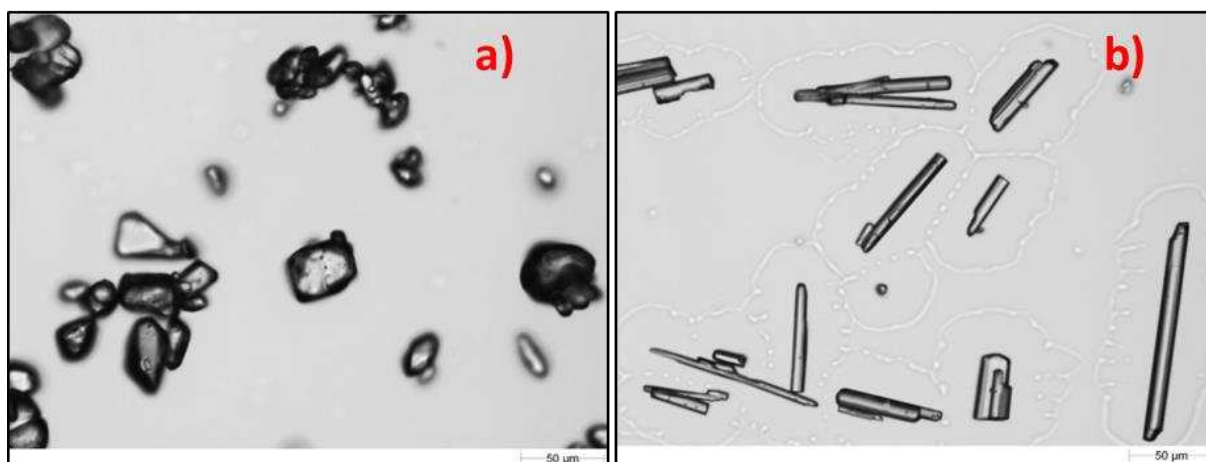
Figure 6 (a) Micrographs of the starting beta phase seeds (b) alpha crystals post transformation experiments

The isotropic nature of the intermolecular bonding and surface chemistry of the beta polymorph with respect to the alpha polymorph, has been previously studied by Rosbottom et al[33] through empirical forcefield modelling and the morphological prediction of these two forms. Drawing upon this study Table 2 highlights the attachment energies[52] and surface saturation[53] for the morphologically important surfaces of the two forms of PABA. Importantly, the alpha polymorph contains high energy and low surface saturation faces in the b needle axis direction associated with the growth of the {0 1 -1} and {1 1 0} surfaces which result in its anisotropic morphology.

Conversely the external morphology for the beta polymorph contains surfaces whereby the attachment energy and surface saturation are more evenly spread across the important particle faces, hence presenting a much more isotropic morphology and arguably a slower dissolution rate relative to the growth rate of the alpha form. Further to this the dominant surface chemistry with respect to surface area for the beta form is dominated by hydrogen bonding interactions, Table 3, whereby solvation of the morphologically important faces would be more isotropic. Whilst alpha PABA also has the slower growing faces dominated by hydrogen bonding resulting in a stable surface, however critically its needle axis and {0 1 -1}

21

surfaces are characterised by π-π stacking interactions which might be expected to result in rapid de-solvation and fast growth. Hence, the observation that dissolution is the rate limiting step in this transformation process can be rationalised in terms of differences in surface area, morphology and surface chemistry between the two polymorphic forms.

Table 3 Attachment energy and % surface saturation for the morphologically important faces of alpha and beta PABA (Adapted from Rosbottom et al [33])

Alpha Polymorph Faces	Attachment Energy (kcal mol^{-1})	% Saturation of surface molecule	Surface Dominant Interaction	Beta Polymorph Faces	Attachment Energy (kcal mol^{-1})	% Saturation of surface molecule	Surface Dominant Interaction
{1 0 1}	−1.7	93.6	H-Bond	{0 1 1}	−10.5	53.8	H-Bond
{1 0 -1}	−10.4	66.2	H-Bond	{0 0 2}	−13.8	39.2	H-Bond
{0 1 -1}	−15.4	35.9	π-π Stacks	{1 0 -1}	−12.2	46.5	H-Bond

Further to this, the nucleation of the stable phase could provide an insight into the observed dissolution rate process. In previous work[37] the kinetics and nucleation mechanism for alpha PABA crystallising from three solvents ethanol, acetonitrile and water, revealed a poly-nuclear nucleation mechanism which was of a more progressive[54] nature in water when compared to ethanol. This is consistent with the formation of a larger number of nuclei in water solutions. This could suggest that the stable alpha solids population will contain a large number of crystals with a large solid-liquid interfacial surface area in comparison to the dissolving meta-stable beta phase which will have a much smaller solid-liquid interfacial surface area, increasingly so throughout the experiement[7]. It should be noted that the experiments described in this work involved seeding compared to the previous nucleation kinetics experiments which were spontaneously nucleated. However these number differences could be influenced by secondary nucleation, reflecting the fact that these experiments are seeded and particle attrition in the magnetically stirred reactor was certainly

likely, hence the quantity of crystal nuclei and a concomitantly greater solid-liquid interfacial surface area of the stable phase could be expected. Overall a combination of these factors supports the observation of a dissolution controlled SMPT of the beta to alpha forms of PABA.

4. Conclusions

The dissolution and growth processes of the SMPT of PABA from its beta to its alpha form have been monitored using in-situ XRD over the temperature range 24°C to 30°C, utilising a new borosilicate capillary transmission flow-through cell designed for in-situ diffraction and or scattering experiments for quantitative analysis of kinetic parameters which govern the phase transformation. This, in combination with in-situ ATR UV-Vis spectroscopy methods, to examine solution concentration, allowed determination of the rate limiting processes during the SMPT. The dissolution of the metastable beta phase was found to fit a zero-order kinetics model, whereas the growth of the stable alpha phase was found to fit a first-order model. The calculated zero order rate constants for dissolution of the beta phase were found to be within the range of 6.80×10^{-4} - 8.17×10^{-5} wt%s^{-1} and 1.00×10^{-3} - 2.50×10^{-4} wt%s^{-1} for the calculated growth rate constants of the alpha phase.

Extrapolation of the calculated growth and dissolution rate constants allowed an estimation of the polymorphic transformation temperature of between 22°C - 24°C. Measurement of the solution absorbance by UV/Vis spectroscopy shows a rapid de-super-saturation suggestive of a dissolution controlled process. This was explained by consideration of the observed particle morphology's of the beta and alpha phase where the isotropic particle morphology of the dissolving beta phase decreases the rate of dissolution relative to the fast growth of the alpha phase which can be linked to its more directional and anisotropic morphology.

This paper has highlighted the value of utilising a combination of flow cell together with in-process XRD and spectroscopy data to provide an insight into the relative balance between the dissolution and growth stages associated with the transformation from the beta to alpha polymorphic forms of PABA by a SMPT process. Ultimately the external particle morphology and surface chemistry of the morphologically important faces for the stable and meta-stable polymorphs of PABA were shown to be significant contributing factors in the overall kinetics which govern this slurry phase transformation.

Associated Content

Supporting information is available, including construction details and commissioning of the new transmission cell together with reproducibility experiments.

Acknowledgements

List of Abbreviations

|	
ATR	Attenuated total reflectance
CPS	Curved position sensitive
FTIR	Fourier transform infrared spectroscopy
PABA	para-aminobenzoic acid
PXRD	Powder X-ray diffraction
SMPT	Solution mediated phase transformation
UV-Vis	Ultraviolet–visible spectroscopy
XRD	X-ray diffraction

List of Symbols

$C_\alpha(t)$	Concentration of the alpha phase at a given point in the reaction
$C_\beta(t)$	Concentration of the beta phase at a given point in the reaction
$C_\alpha(f)$	Concentration of alpha phase formed at the end of the reaction
$C_\beta(i)$	Initial starting concentration of the beta phase
$k_{g\alpha}$	Growth rate constant with respect to the alpha polymorph
$k_{d\beta}$	Dissolution rate constant with respect to the beta polymorph
wt %	Weight percent
$X\alpha$	Fractional conversion of the alpha phase solids
$X\beta$	Fractional conversion of beta phase solids

For Table of Contents Use Only

Kinetics of the aqueous-ethanol solution mediated transformation between the beta and alpha polymorphs of para-aminobenzoic acid

Thomas D. Turner*, Steve Caddick, Robert B. Hammond, Kevin J. Roberts and Xiaojun Lai

Graphical Abstract
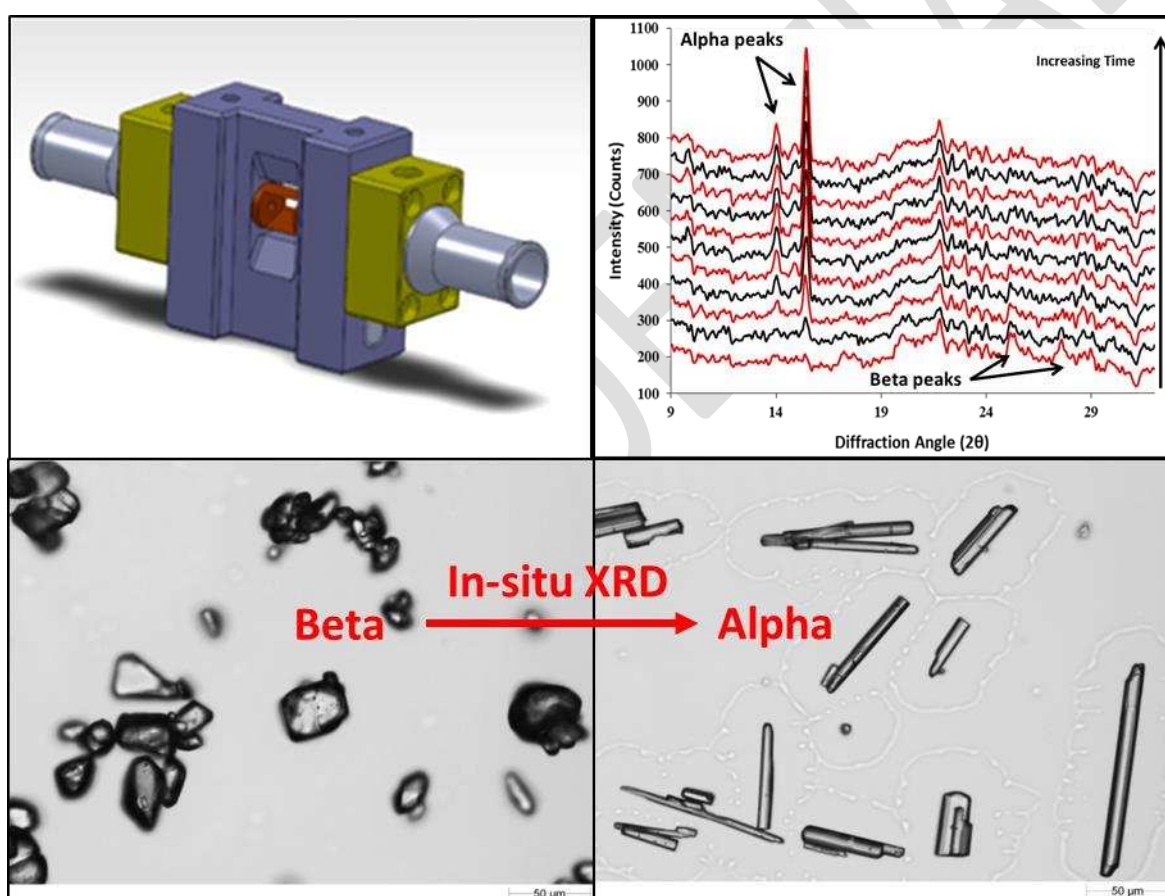
Synopsis

This work presents the development of a new in-situ X-ray transmission flow cell system and its application in the determination of the polymorphic transformation kinetics for para-aminobenzoic acid.

References and Notes

1 Byrn, S. R.; Pfeiffer, R.R.; Stowell, J. G. Solid State Chemistry of Drugs, **1999,** 2nd edn SSCI Press

2 Bernstein, J. Polymorphism in molecular crystals, **2002**, Vol. 14, Oxford University Press

3 Lee, A., Y.; Erdemir, D.; Myerson, A., S. Annu. Rev. Chem. Biomol. Eng. **2011**, 2, 259

4 Bauer, J.; Spanton, S.; Henry, R.; Quick, J.; Dziki, W.; Porter, W.; Morris, J.; Pharm. Res. **2001**, 18, 859

5 Dunitz, J. D.; Bernstein J. Acc. Chem. Res. **1995**, 28, 193

6 Gu, C.; Young, V. Jr.; Grant, D. J. W. J. Pharm. Sci. **2001**, 90, 1878

7 O'Mahony, M. A.; Maher, A.; Croker, D. M.; Rasmuson Å. C.; Hodnett, B. K. Cryst. Growth Des. **2012**, 12, 1925

8 Wantha, L.; Flood, A. E. J. Cryst. Grow. **2013**, 362, 66

9 Helmdach, L.; Feth, M. P.; Ulrich J. Org. Process Res. Dev. **2013**, 17, 585

10 Hu, Y.; Liang, J. K.; Myserson, A. S.; Taylor, L. S.; Ind. Eng. Chem. Res., 2005, 44, 5,

11 Herman, C.; Haut, B.; Douieb, S.; Larcy, A.; Vermylen, V.; Leyssens, T.; Org. Process Res. Dev. **2012**, 16, 49

12 Hu, Y.; Wikstrom, H.; Byrn, S. R; Taylor, L. S. J. Pharm. Biomed. Anal. **2007**, 45, 546

13 Qu, H.; Munk, T.; Cornett, C.; Wu, J. X.; Bøtker, J. P.; Christensen, L. P.; Rantanen J.; Tian F. Pharm. Res. **2011**, 28, 364

14 Ono, T.; ter Horst J. H.; Jansens P. J. Cryst. Growth. Des. **2004**, 4, 465

15 Scholl, J.; Bonalumi, D.; Vicum, L.; Mazzotti, M. Cryst. Growth. Des. **2006,** 6, 881

16 Craig, S. R.; Roberts, K. J.; Sherwood, J. N.; Sato, K.; Hayashi, Y.; Iwahashi, M.; Cernik, R. J. J. Cryst. Grow. **1993**, 128 1263

17 Cernik, R. J.; Craig, S. R.; Roberts, K. J.; Sherwood, J. N.; J. Appl. Crystallogr. **1995**, 28, 651

18 MacCalman, M. L.; Roberts, K. J.; Hendriksen, B. Proceedings of the 5th World Congress of Chemical Engineering **1996**, 698

19 MacMillan S. D.; Roberts, K. J.; Rossi, A.; Wells, M. A.; Polgreen, M. C.; Smith, I. H. J. Cryst. Growth. Des **2002,** 2, 221

20 Gron, H.; Mougin, P.; Thomas, A.; White, G.; Wilkinson, D.; Hammond, R. B.; Lai, X.; Roberts, K. J. Ind. Eng. Chem. Res. **2003**, 42, 4888

21 Hennessy, A.; Neville, A.; Roberts, K., J. J. Cryst. Growth Des. **2004**, 4, 1069

22 Craig, S., R.; Hastie, G., P.; Roberts, K., J.; Sherwood, J., N.; Tack, R., D.; Cernik, R., J. J. Mater. Chem. **1999**, 9, 2385

23 MacCalman, L. M.; Roberts, K. J.; Kerr, C.; Hendriksen, B. J. Appl. Crystallogr. **1995**, 28, 620

24 MacMillan, S. D.; Roberts, K. J.; Wells, M.; A.; Polgreen, M. C.; Smith, I. H. J. Cryst. Growth Des. **2003**, 3, 221

25 Alison, H. G.; Davey, R. J.; Garside, J. Quayle, M. J.; Tiddy, G. J. T.; Clarke, D. T.; Jones, G. R. Phys. Chem. Chem. Phys. **2003**, 5, 4998

26 Takahashi, H.; Iwama, S.; Clevers, S.; Veesler, S.; Coquerel, G.; Tsue, H.;Tamura, R.; Cryst. Growth Des. **2017**, 17, 671

27 Davis, T. D.; Morris, K. R.; Huang, H.; Peck, G. E.; Stowell, J. G.; Eisenhauer, B. J.; Hilden, J. L.; Gibson, D.; Byrn, S. R. Pharm. Res. **2003**, 20, 1851

28 Dharmayat, S.; Hammond, R. B.; Lai, X.; Ma, C.; Purba, E.; Roberts, K. J.; Chen, Z.; Martin, E.; Morris, J.; Bytheway, R.; Crys. Growth Des. **2008**, 8, 2205

29 Lai, T., F.; Marsh, R., E. Act. Cryst. **1967**, 22, 885

30 Alleaume, M.; Salascim, G.; Decap, J. Comptes Rendus Hebdomadaires Des Seances De L Academie Des Sciences Serie C, **1966**, 262, 416

31 Gracin, S.; Rasmuson, A., C. Cryst. Growth Des. **2004**, 4, 1013

32 Hao, H.; Barrett, M.; Hu, Y.; Su, W.; Ferguson, S.; Wood, B.; Glennon, B. Org. Process Res. Dev. **2012**, 16, 35

33 Rosbottom, I.; Roberts, K. J.; Docherty, R.; Cryst. Eng. Comm. **2015**, 17, 5768

34 Sullivan, R. A.; Davey, R. J.; Sadiq, G.; Dent, G.; Back, K. R., ter Horst J.; H., Toroz, D.; Hammond, R., B. Cryst. Growth Des. **2014**, 14, 2689

35 Toroz, D.; Rosbottom, I.; Turner, T. D.; Corzo, D. M. C.; Hammond, R. B.; Lai, X.; Roberts, K. J. Faraday Discuss. **2015**, 179, 79

36 Sullivan, R. A.; Davey, R. J. Cryst. Eng. Comm. **2015**, 17, 1015

37 Turner, T. D.; Corzo, D. M. C.; Toroz, D.; Curtis, A.; Dos Santos, M. M.; Hammond, R. B.; Lai X.; Roberts, K. J. Phys. Chem. Chem. Phys. **2016**, 18, 27507

38 http://www.julabo.com/

39 https://www.bruker.com/

40 Hammond, R., B.; Lai, X.; Roberts, K. J.; Thomas, A.; White, G. Cryst. Growth Des. **2004,** 4, 943

41 Calderon de Anda, J. A.; Hammond, R. B.; Lai, X.; Roberts, K. J.; Wang, X. Z. J. Cryst. Growth. **2006**, 294, 35

42 http://www.inel.fr

43 http://www.jvsemi.com

44 http://www.watson-marlow.com

45 Zeiss (2017) www.zeiss.co.uk/corporate/en_gb/home.html

46 http://www.jvsemi.com/

47 http://www.ni.com/labview/

48 Chen, Z. P.; Morris, J.; Martin, E.; Hammond, R. B.; Lai, X.; Ma, C. Y.; Purba, E.; Roberts, K. J.; Bytheway, R. Anal. Chem. **2005**, 77, 6563

49 Svard, M.; Nordstrom, F. L.; Hoffmann, E.; Aziz, B.; Rasmuson, Å. C. Cryst. Eng. Comm. **2013**, 15, 5020

50 Cardew, P. T.; Davey, R. J. Proc. R. Soc. London. **1985**, 415, 28

51 Wantha, L.; Flood, A. E. Chem. Eng. Tech. 2013, 36, 1313

52 E_{att} (hkl) = E_{Cr} − E_{slice} (hkl) where E_{Cr} is the crystal lattice energy and E_{slice} (hkl) and E_{att} (hkl) are respectively the slice (related to surface stability) and attachment (related to surface binding) energies.

53 Surface saturation = E_{slice} / E_{Cr} and is a measure of how many of the bulk (intrinsic) intermolecular interactions (synthons) are still saturated by surface termination, i.e. the larger the value the more stable the surface.

54 Kashchiev, D.; Borissova, A.; Hammond, R. B.; Roberts, K. J. J. Cryst. Growth. **2010**, 312, 698

55 Turner, T. D.; Molecular Self-Assembly, Nucleation Kinetics and Cluster Formation Associated with Solution Crystallisation, Ph.D. Thesis, University of Leeds, England, 2015